MAGIC-TDAS 04-03
Martin Merck

Report on the Chess-boarding of the Mirrors and AMC Improvements done during the July 2004 Intervention

Adrian Biland, Markus Garczarczyk and Martin Merck

Figure 1: The MAGIC telescope with fully assembled mirror panels (August 2004)

Contents

Chapter 1

Rearrangement of mirror panels

Every period we mounted new panels and focused the mirrors with the Roque-Lamp we observed an continuous defocussing of individual mirrors on panels. To improve the PSF it was necessary to fine focus this mirrors everytime again. The reason for the defocussing were not enough space between panels. During the movements of actuators panels touched neighbor mirrors and defocused. Specially when the actuators were centering, going from the lower to the upper endswitch, the consequence become dramatic. This is the reason why it was not allowed the use the centering procedure in the AMC software anymore, but even then colliding of mirrors was not fully excluded.

The only solution to avoid this collisions was to rearrange the panels to chess-board structure as shown in figure 1.1.

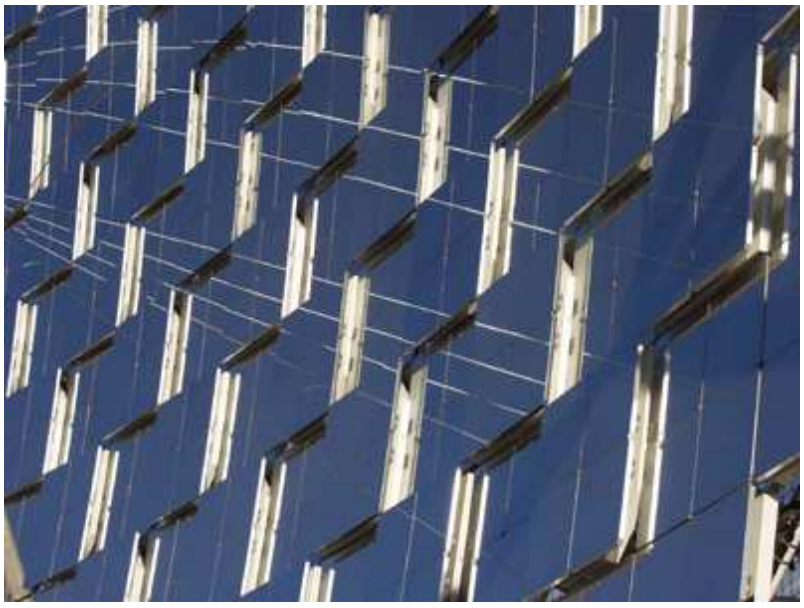

Figure 1.1: Chess-board structure of the panels on MAGIC telescope.

1.1 Chess-board arrangement of mirror panels

First of all we would like to thank the collaborators from Barcelona, Munich, Padova, Zurich and Lodz which gave us support in form of man power for the rearrangement of the panels.

Figure 1.2: Team working on the chess-board structure. From left: Andreas Wenger, Urs Horisberger, Mauro Negrello, Thomas Rauber, Peter Sawallisch, Massimo Rebeschini, Marco Burkert, Markus Garczarczyk, Davide Aggugiaro and Jan Rachowski (who's dedicated task was to replace the motor connectors on the AMC boxes). Missing on the picture are: Jose Ferrer and Rheinhard Hofmann.

To arrange panels in chess-structure we produced 30 mm thick Al blocks in the workshop of MPI. To rise panels we mounted the Al blocks under the three mounting points which fix the panel to the carbon-fiber-tube structure. We were trying to achieve a 40 mm distance between mirrors of different panels. This is the space we are sure that mirrors don't collide with the neighbors.

In the first step we tried to follow the suggestion presented during the collaboration meeting in Tuorla. The idea was to make the chess-board structure only in the central part of the telescope dish and rise in total 64 panels.

During this installation we realized that even in the outer region where more space should be available for the panels, it was not possible to find a collision-free arrangement. After long trials we decided to arrange all panels in chess-board structure as shown in figure 1. Finally we raised 118 panels.

Additionally the last 21 panels have been mounted and the dish is **finished** now!

1.2 Parabolic form of the reflector after the chess-board arrangement

In order to prove the overall shape of the reflector we measured with special laser instrument the distance between the mirror surface and the center of the lids for

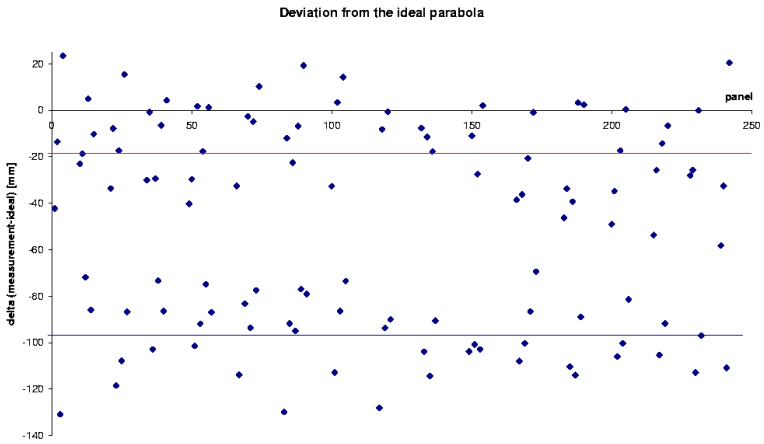

Figure 1.3: Plot of the deviation of individual panels from the optimal focal length.

each individual panel. These measurements had to be done from the cherry-picker, so it was not possible to reach the upper half of the dish. To measure these panels it would be necessary to rotate the dish to zenith -70 deg. Since at that time, the fine focussing of all mirrors and panels had already been accomplished (taking more than 3 nights!), it seemed to risky to rotate over zenith and possibly introduce some irreversible changes of the alignment. Anyhow the dish should be symmetric and differences between upper and lower part are expected to be negligible (but it would be nice to measure it sometime).

Figure 1.3 show the difference between the measured and optimal focal length for each individual panel. The measured distance is corrected for the offset from the camera lid until the Winston-Cone plane. There are two regions on the plot. The region around -20 mm corresponds to the lower- and the region around -100 mm corresponds to the higher panels of the chess-structure. From this measurement we get the mean distance of 80 mm between the two layers of the chess-structure.

The Figure 1.4 show the measurement of the lower part of the telescope dish. Here the chess structure is visible (blue colour corresponds to raised panels). Panels in the outer ring (green colour) are in the optimal distance for the parabolic shape, adjusted before the MAGIC camera was mounted. The offset of -40mm is due to wrong distance between the MAGIC camera and the optimal focal length for individual mirrors.

1.3 Rebalancing the telescope

Since more panels have been added and the Camera moved 3cm further away from the dish to gain space for the installation of the inner LEDs and curtain, it was

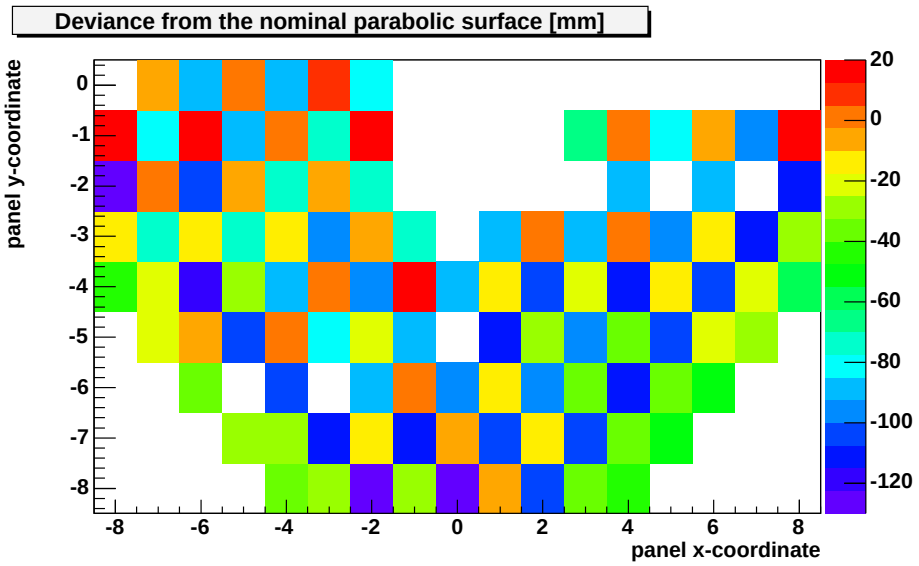

Figure 1.4: Plot of the laser measurements for the panels on the lower part of the dish.

needed to modify the counterweight to get the telescope balanced again. When the Camera is in Roque-Lamp position, the telescope is perfectly balanced; this means when the Camera is moved to '10km' of 'infinity' position (i.e. closer to the dish), the telescope will tend to rotate to zenith orientation in case of complete loss of power and none working brakes.

Chapter 2

Improvements to the AMC

2.1 Installation of a projection screen on the lids

To improve the determination of the laser spot position on the camera lid a flat projection screen is necessary. Since the lids feature a frame on the borders and the frame profiles overlap in the central part of the lids, the surface is not plane which makes it very difficult to get precise laser positions.

A plane screen was proposed already during the Wuerzburg meeting in 2002 and accepted from SC. Since nobody made an effort to build this projection screen we decided to make them by ourself.

We used two 2mm thick Al plates with the size of 500x250 mm. Each plate is mounted on 9 mm long spacebars and fixed with four M4 screws to the lid. For the screws we mounted small rivets on the lid front side. We made sure that everything stayed watertight.

The projection screen is painted with matt white colour to avoid reflections of the lasers from the mirrors.

Figure 2.1: The two Al-plates mounted on the camera lids acting as a projection screen for the lasers of the AMC.

2.2 Definition of the Roque-Lamp pointing

We defined a new Roque-Lamp position as the added weight of new mirrors and counterweights since October may have affected the structure of the telescope. To determine the exact pointing position of the telescope for the Roque-Lamp we removed the backside of the camera and used the small telescope mounted on the frame to find the Roque-Lamp by looking through the hole left by the not installed central pixel. In table 2.1 we compare the new positions obtained with the old values used since October 2003. The shaftencoder positions agree reasonably well with the old positions. SE-Zd1 shows some strange behavior as it may display 1301 or $1301 + 2^{14} = 1301 + 16384 = 17685$.

Table 2.1: Coordinates of the Roque-Lamp before and after chess-boarding.

	Old	New
SE-Az	29694	29691
SE-Zd1	1301	1301 / 17685
SE-Zd2	9909	9912
Zd	75 36' 00"	76 18' 36"
Az	151 12' 00"	149 54' 48"

The zenith distance Zd and azimuth Az have changed considerably, due to the new pointing model. We give them in this table as they are needed to point the telescope to the Roque-Lamp. As Cosy still does not implement the possibility to point the telescope using shaft encoder values, users have to enter the zenith distance and azimuth to move the telescope to the desired position. As the pointing model is changing regularly, it is imperative to check the shaft encoder positions after the telescope stopped moving and correct the pointing using the manual control until the right shaft encoder positions have been reached.

2.3 Mounting a temporary CCD for Fine-focusing

The four mirrors on each panel can not be moved remotely. Therefore it is needed to move them manually to an orientation in which all four reflect the light to the same position. This is achieved by defocusing all panels but one, using the AMC. In this scenario the reflection of the Roque-Lamp from each individual mirror on the single focused panel can be identified and corrected. So far this had been done by using one of the CCDs mounted in the center of the dish. The resolution and sensitivity of this CCD did limit the precision that could be reached.

To improve this, a special 5m long mast carrying a CCD was temporarily mounted on the Camera (the mast can be seen on Fig. 1). Since this CCD was much closer to the reflection screen a significantly higher resolution was available. Therefore it was possible to do the fine focusing of the mirrors better than before. A limiting factor was the small dynamic range of the used CCD: specially the corner mirrors showed much fainter signals. Since it was extremely time consuming to change the

aperture of this CCD it was unavoidable that some mirrors were much overexposed while others almost invisible. Another problem was that the rechargeable battery of the new Roque-Lamp only lasted for 4 hours and it was not possible to find suitable batteries on La Palma.

The same CCD was also used to find the optimal position of each panel.

After the focusing was finished, the mast and CCD have been removed again.

2.4 New LED positions

During the camera access the AMC LED-housings have been changed. During this operation the LEDs have been remounted onto the camera lid at slightly different positions than previously defined. We therfore had to newly determine the default position of the LEDs. This has to be done in a defined position. We decided to use the Roque-Lamp position as the default.

The new LED positions were found using the AMC software and the better spot finding algorithm described in section 2.6.

Table 2.2: Position of the AMC LEDs when the telescope is pointing to the Roque-Lamp.

	X	Y
LED 1	105.92	75.65
LED 2	560.30	66.15
LED 3	111.30	418.13
LED 4	564.68	408.78
Camera center	304.00	239.20

To find the center of the camera, we tried to use a flash light inside the central pixel and to determine the position by the program like it is done for the LEDs. However this was only possible in the camera access position of the telescope, whereas our reference frame is defined by the Roque-Lamp position. Furthermore it was not possible to get a stable accurate spot position with the flashlight. We then decided to use a mean of the flashlight positions and the visual center of the camera as seen during daylight with the video camera.

This means that the reference optical axis may not correspond exactly to the geometrical center of the telescope camera. As this is one of the effects corrected by the pointing model, we prefer to leave the exact correction of the optical axis to the T-Point correction algorithm.

2.5 Determination of the AMC CCD camera scale

We measured the distances between the LEDs on the camera LID and used this measurement together with the images of the LEDs on the AMC CCD camera to

determine the scale of the CCD video pixel. Each pixel corresponds to 2.27 mm on the camera plane, or each mm corresponds to 0.44 CCD pixels.

2.6 Improved spot finding algorithm

To improve the Spot finding algorithm the calculations have been changed from integer to floating point calculations. The spot position is now stored in floating point accuracy with 2 decimal digits. The calculation is based on a weighted mean, with weights corresponding to the signal from the CCD camera (intensity of the laser spot / LEDs). In theory a precision of 0.1 or better should be obtainable. However due to movements of the camera this accuracy is not expected to be achievable. Tests showed good reproducibility at the 0.2 CCD pixel level in low wind conditions. At higher wind speeds the reproducibility was reduced to 0.3 CCD pixels. This will allow us to focus the mirror spot with a precission of better then 1 mm on the camera plane, compared to 5 mm with the old setup.

2.7 Changes to the panel-movement calibration

During the calibration procedure after the chess-boarding of the mirror panels, lots of panels showed a bad fit as the linear regression through a line parallel to the Y-axis gives unstable results. The correlation coefficient R of the regression also gives a very low value, as the used model $y = a + bx$ is not anymore describing the curve very well.

To solve this problem, we reverse the axis after the calibration if the correlation coefficient $R < 0.5$. This means the Y-axis becomes the X-axis and viceversa. In this situation the curve becomes $y \approx const$ and the fitted line gives a much better result. To indicate this axis reversal the format of the file "PanelPos.txt" was changed to include a flag for the axis reversal. All procedures inside the AMC software where changed to handle the reverse axis if necessary.

We want to emphasize here that this axis reversal could not be tested thoroughly and may have still some unexpected effects. This means that if panels are re-calibrated a thorough test of the resulting calibration is needed.

2.8 Analysis of communication problems

We performed an analysis of the communication problems after the resistor on the RS-485 chip had been changed in all boxes. A quite low error rate was detected for most panels. Only very few so called 0x80 or 0x0A errors remained. This type of error was already traced to a missing delay in the AMC controller card software when switching from the receiver state to the sender state. A fix made in March showed that this type of errors could be removed totally by introducing this delay in the Atmel AVR microcontroller software. However, the two RS-485 lines to which the controllers are connected, which had the bootloader installed (and this delay issue fixed) showed much higher error rates (factor 3-5) then the other lines. These errors

were all of a new type where part of the response of the microcontroller gets lost due to a too long delay between send characters. To reduce the error rate we decided to remove the bootloader and install the default software onto these cards. After this reprogramming the tests still showed a high error rate on these two lines. We finally decided to get the flash image from a low error rate card and install this same flash image on the high error rate cards. After this procedure all microcontrollers showed a low communication error rate.

The problem was then traced to a new version of the AVR C-compiler (CodeVision AVR) which was installed early this year. This new compiler seems to optimize the generate code in such a way that it breaks the timing of the custom implemented comunication protocol. In La Palma we could not find an old functioning version of the compiler, to verify this hypothesis, but all test indicate that the compiler is the cause of the timeout problems.

This problem is more serious than expected. The missing delay in switching between sending and receiving maybe solved using an old compiler version and thus the communication problems may be finally solved. However, the used microcontroller ATmega163 is not in production anymore and the newly produced spare cards use a new, pin compatible, microcontroller (ATmega16). The software of this new microcontroller is nearly identical to the old software, but to program this chip the new compiler version is necessary. During our stay in La Palma it was not possible to get one of the new cards working with a low error rate. Currently all available ATmega163 controller boards are installed in the telescope with no old card remaining as a spare.

A solution to this problem is urgently needed!

2.9 Corrections to the focusing procedure

Our default focusing procedure uses the Roque-Lamp at a distance of 980m to focus the individual mirror panels on a screen in front of the plexiglass window of the camera. We used during this focusing campaign a 5mm thick styropore screen on which we fixed a paper with an image of the hexagons of the central pixels. After this procedure, we close the camera lid and save the laser spot positions on the camera lid and the motor steps, relative to the centered value. During a laser adjustment procedure, we determine the position of the laser spot on the camera lid and calculate the needed motor steps to move the mirror and thus the laser spot until it agrees with the stored position.

This procedure introduces two main errors

1. The focal plane we used for the Roque-Lamp adjustment does not correspond to the focal plane of the camera, even if the camera was moved to Roque-Lamp focus position. This is due to the fact, that the focal plane of the camera (upper plane of the Winston-Cones) is 3 cm behind the top of the plexiglass window. In addition we have to add the 0.5 cm of the thickness of the styropore screen used to fix the reference plane. In total the two focal planes are apart 35 mm. In figure 2.2 we show the effect of this error for each individual mirror panel.

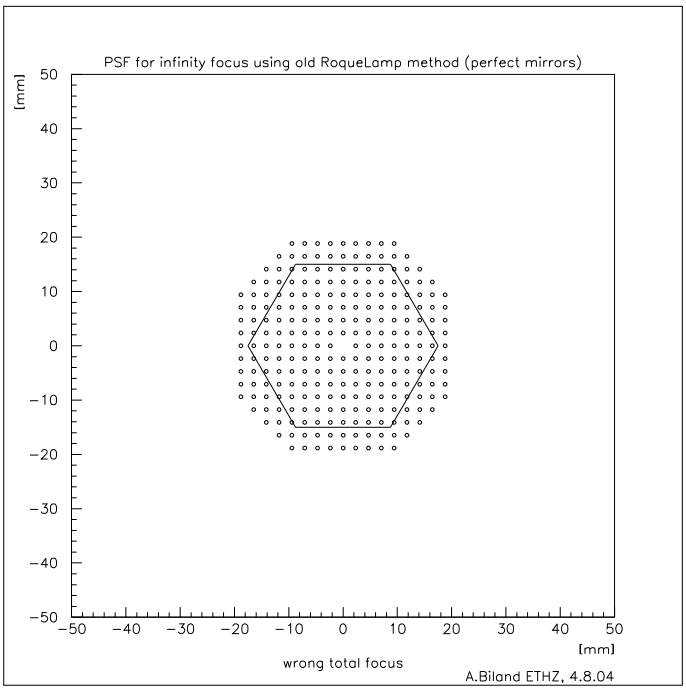

Figure 2.2: Error introduced by the distance of the Roque focusing plane to the real camera focal plane defined by the winston cones. Each point shows the displacement for one mirror panel.

For comparison we also indicate the size of the central pixel. The effect is linear to the distance of the mirror panel from the optical axis.

2. In contrast to a sphere, a parabola can only focus an image at infinity. Images of nearer objects can only be focused by ellipses where the object is in one focal point and the image in the opposite focal point. As the mirror dish is parabolic we can't deform it to the needed ellipse when focusing to the Roque-Lamp at 980 m distance. The effect of a parabolic mirror imaging a finite distance object is that all points on the mirror surface with different distances from the optical axis have different focal lengths. So, whereas a mirror segment just in the center of the dish would have a focal length of 17300 mm a panel at the edge of the mirror with a distance of the center of the panel to the optical axis of 8 m has a focal length of 17334.3 mm.

   The effect introduced by this error on the PSF is shown in figure 2.3. For central mirror panels the effect is quite small, but at larger distances from the optical axis the effect becomes comparable to the PMT-camera pixel size.

   Both effects add linearly and make an error in the same direction, thus increasing the total error. The total effect on the PSF is illustrated in figure 2.4.

The first effect could be corrected by redefining the Camera position in a way the difference between 'Roque-Lamp' and 'infinity' position is enlarged by another 35 mm. To achieve this, some hardware modifications would be needed. But the

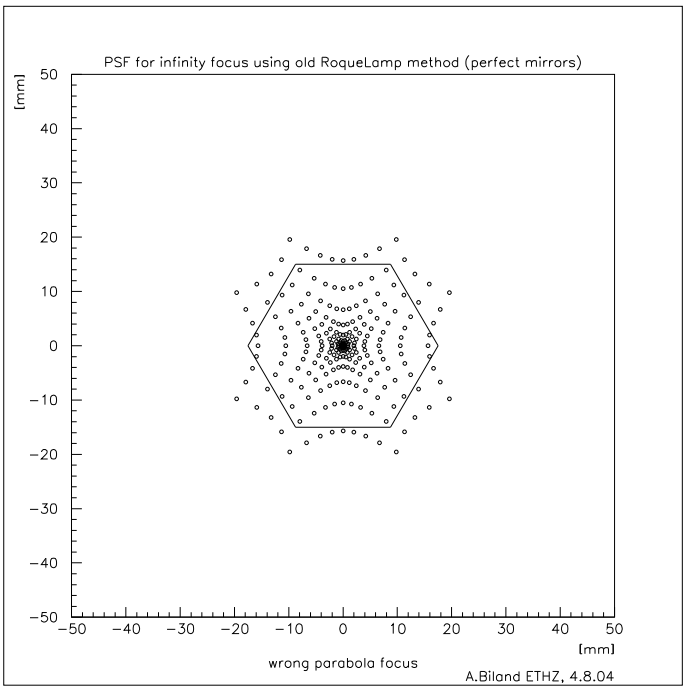

Figure 2.3: Error introduced by using the different focal length of a parabola if not focused to infinity. Each point shows the displacement for one mirror panel.

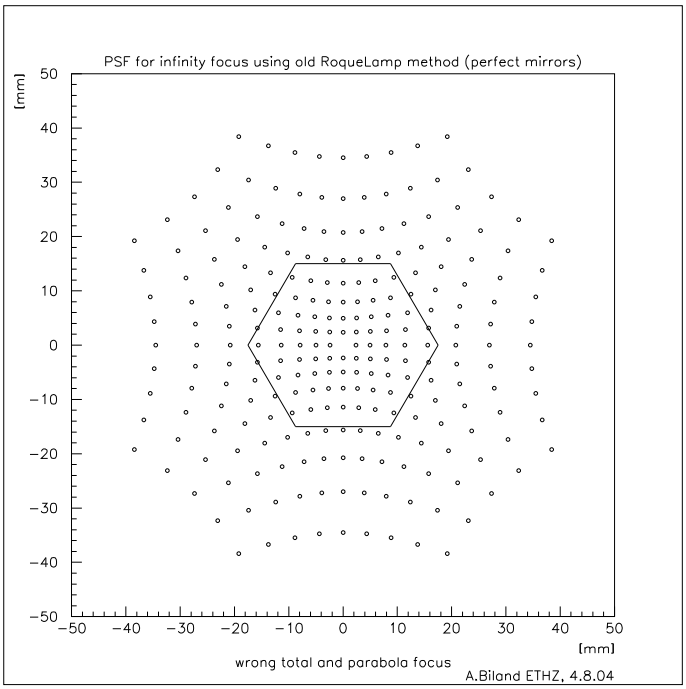

Figure 2.4: Total error in the PSF introduced by the two previous errors. Note that both errors add up linearly and are in the same direction. Each point shows the displacement for one mirror panel.

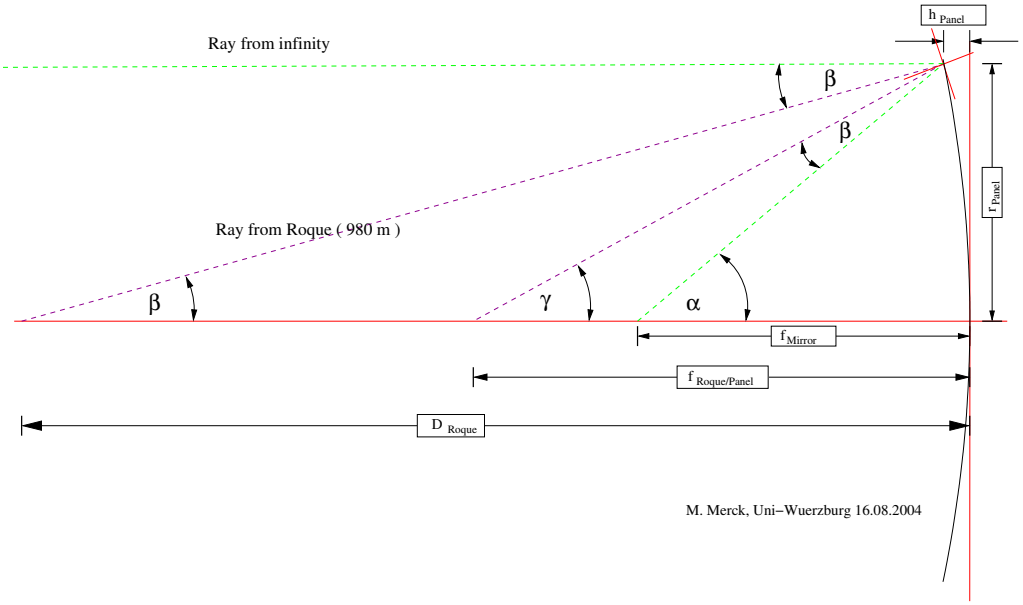

Figure 2.5: Illustartion of the focusing procedure with the Roque Lamp.

second effect by definition can not be corrected be Camera movements. Therefore we decided to correct both effects by modifying all the panel orientations via AMC accordingly. Two slightly different algorithms where implemented by Adrian and Martin to calculate the magnitude of the effect of the parabolic shape on the PSF. Both gave the same result.

In figure 2.5 we explain the correction needed for the parabolic shape of the mirror. A ray from infinity will be focused to the focal point of the parabola as shown. A ray from a finite distance, like the Roque Lamp, will be focused to a point at a greater focal distance. (This is always true not only for a parabolic mirror shape but also for the spherical mirror shape (Davis-Cotton design)).

In figure 2.5 we use the following definitions:

- f_{Mirror} : Focal length of the parabola (17000 mm).
- D_{Roque} : Distance to Roque Lamp (980000 mm).
- r_{Panel} : Radial distance of a individual mirror panel from the dish center .
- h_{Panel} : Height of the panel above the tangential Plane of the mirror dish.
- α : Angle at which a ray from infinity, reflected from a panel at radius r_{Panel}, intersects the optical axis in the focal point. Angle at which a panel at radius r_{Panel} sees the Roque Lamp.
- β : Angle at which a panel at radius r_{Panel} sees the Roque Lamp.
- γ : Angle at which a ray from the Roque Lamp, reflected from a panel at radius r_{Panel}, intersects the optical axis in the focal point.

From the figure 2.5 we can calculate the angles α, β and γ using the following equations:

$$\alpha = \arctan\left(\frac{r_{Panel}}{f_{Mirror} - h_{Panel}}\right) \tag{2.1}$$

$$\beta = \arctan\left(\frac{r_{Panel}}{D_{Roque} - h_{Panel}}\right) \tag{2.2}$$

$$\gamma = \alpha - \beta \tag{2.3}$$

The focal length for a panel when focusing to the Roque Lamp is now given as:

$$f_{Roque} = \frac{r_{Panel}}{\tan(\gamma)} + h_{Panel} \tag{2.4}$$

The height of the Panel can be calculated using the formula for the parabola:

$$y^2 = 4\,a\,x \tag{2.5}$$

where a is the distance from the vertex to the focal point or the focal length.

Now the height is calculated as:

$$h_{Panel} = \frac{r_{Panel}^2}{4\,f_{Mirror}} \tag{2.6}$$

Using this equation the new focal distance can be calculated for an arbitrary panel at a radial distance r_{Panel}. During the focusing with the Roque-Lamp we shift the camera back by 300.1 mm thus changing the focal length to 17300.1 mm. This corresponds to the exact change needed for a spherical mirror, as in this circumstance all panels would have the same focal length. For the parabola the focal length of each panel will depend on the radial distance of this panel from the mirror dish. As we force it in the procedure to focus at 17300.1 mm we have to correct for the difference in focal length for that panel compared to the 17300.1 mm. This is shown in figure 2.6.

The correction is now calculation by simple rule of three to:

$$\frac{Corr}{df_{Roque}} = \frac{r_{Panel}}{\left(f_{Roque/Panel} - h_{Panel}\right)} \tag{2.7}$$

In a similar easy calculation by rule of three the correction for the difference in focal plane to the plane of the winston cones can be calculated:

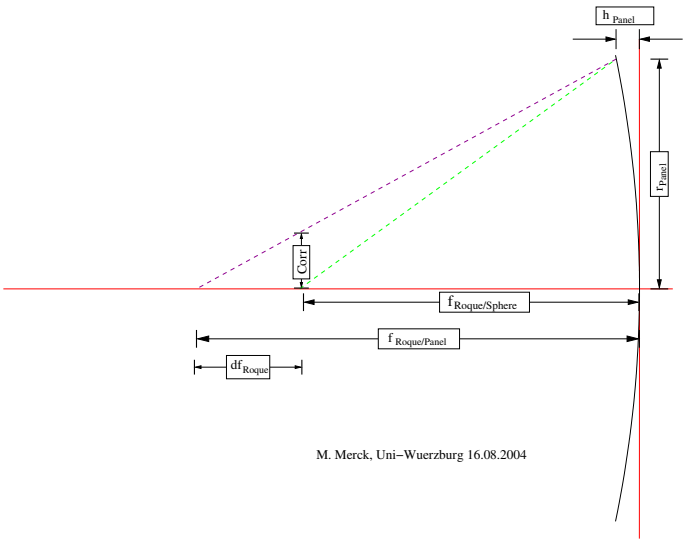

Figure 2.6: Correction due to parabolic shape of the mirror.

$$\frac{Corr2}{d_{WinstonCones}} = \frac{r_{Panel}}{\left(f_{Roque/Panel} + d_{WinstonCones} - h_{Panel}\right)} \tag{2.8}$$

where $d_{WinstonCones}$ is 35 mm.

The AMC software was updated to correct for this errors. First of all the magnitude of the shift of the focal spot on the focal plane is calculated for each panel using the panel center projected on a plane, as the distance to the optical axis (This procedure still introduces a small error as the distance of the panels from each other on this plane is not 1000mm but depends on the parabolic shape of the mirror). In a second step the reference laser positions stored for each panel are corrected by half of the displacement needed for the mirror spot as calculated above. (A movement of the laser on the camera plane corresponds always to a movement of the image spot by double this magnitude). The mirrors are now adjusted during the laser adjust procedure to the new reference position.

2.10 Other AMC enhancements

We also introduced some other small changes to the AMC software.

Most important, the AMC software and all files used by the AMC are now managed over the CVS repository. In this way old revisions of the AMC software and the configuration files (like Panels.txt and PanelPos.txt) are always available. This change has the side effect that the location of the AMC program has changed. The actual versions of program and configuration files are located in the AMC subdirectory of the amc users home directory. Inside this directory, the directory activemirrorcontrol contains the KDevelop project and all subfolders of the main

AMC program. In the directory share/amc the configuration files, lookup tables and icons of the application are stored.

Other changes include the graphical indication of the selected panel and a graphical view of all panels with the lasers being turned on. The program version number and the build date/time are also indicated on the main AMC window. Some adjustment had also to be done to account for the changed format of the report send by central control.

All this changes don't affect the operation of the AMC software. To start the program you still have to type 'amc' in any terminal of pc7.

2.11 Relocation of the AMC computer

We moved pc7, dedicated for the AMC, from the Wuerzburg container to the counting house. The necessary cabling of the data and video cabels has also been carried out.

Chapter 3

First results with the new focusing

3.1 Focus achieved after the panel rearrangement

After the rearrangement of the mirror panels to the chess-board configuration, we had to recalibrate all panels and redo the Roque-Lamp focusing procedure. After focusing all panels for the Roque-Lamp we restarted the program, reinitialized all panels, defocused all panels and refocused them using the stored motor positions.

We took some images of the resulting PSF which are shown in figure 3.1. You can nicely see that most of the light is concentrated inside the hexagon drown on the focusing screen, showing the size and location of the central pixel.

Fitting a 2-dimensional gauss with constant background and allowing for saturation

$$g(x,y) = \min(255., N\ e^{(-0.5(\frac{x-x_0}{\sigma})^2 - 0.5(\frac{y-y_0}{\sigma})^2)} + BG) \tag{3.1}$$

to the central regions of figure 3.2 b) and c) shows that the 2σ-curve corresponds approximately to the border of the central pixel. This means that under best circumstances we can expect 90-95% of the light to be within one pixel. What PSF we reach under real conditions has to be checked from star-images and muon-rings.

3.2 Comparison of the effects compensated in the new AMC program

To test the improvements achieved with the new focusing procedure and the corrections implemented in the AMC program we moved the camera back to its nominal focusing at 10 km. We lowered the ETH curtain, which should be located at 3 cm from the winston cone plate and thus correspond to infinity focusing.

We first selected Vega (a 0 mag star) as our test candidate and pointed the telescope to this star. After setting the mirror panels to the stored Roque-Lamp position, we used the POINTING video camera and made an image, integrating 50 video frames. In figure 3.3(a) the resulting spot on the curtain can be seen.

In a next step we focused the mirror using the old laser adjustment procedure. In figure 3.3(b) we can clearly see some improvement but the image is still quite blurred. We now turned on the correction for the 35 mm focal plane shift. The result is shown

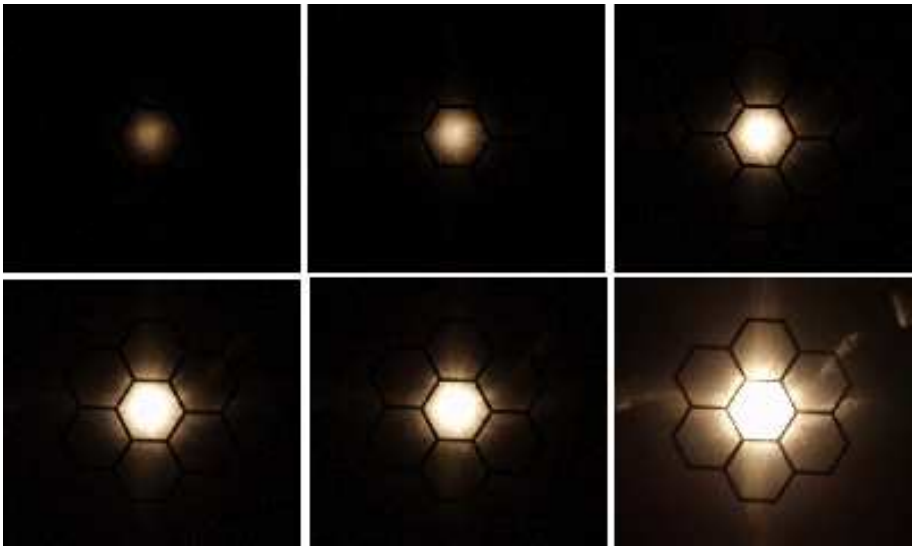

Figure 3.1: Images made with digital photo camera one meter in front of the paper used for focussing with the Roque-Lamp. The six images were made with different exposure times ranging from tenth of a second (upper left picture) up to two seconds (lower right picture). At the 3rd picture the image is already in saturation.

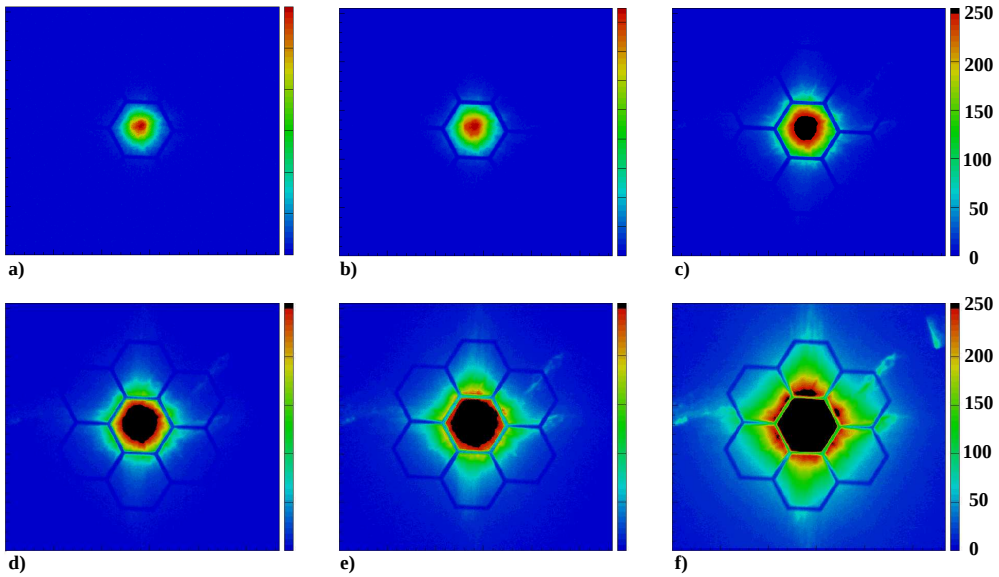

Figure 3.2: Images from figure 3.1 shown as histograms. From this plots the saturation of the digital camera is clearly visible.

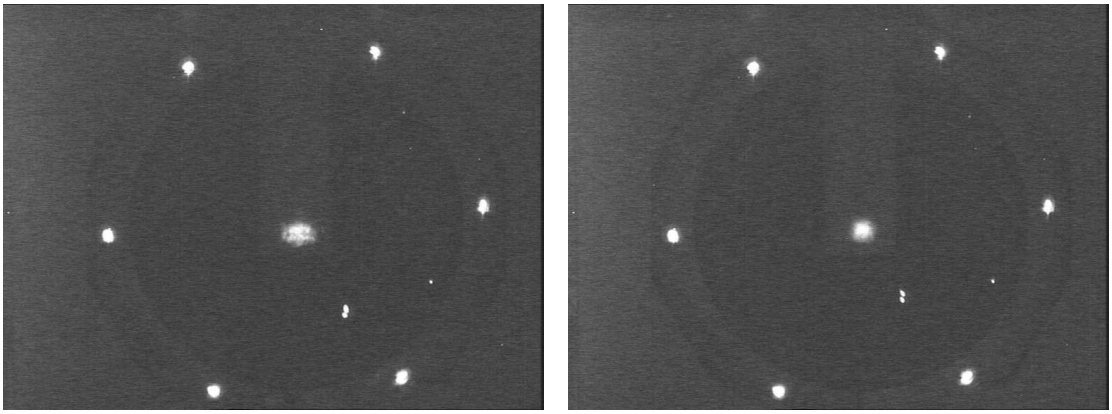

(a) After initialization to Roque-Lamp positions

(b) After laser adjustment

(c) After correcting for wrong focal plane

(d) After correcting for parabolic effect and focal plane

Figure 3.3: Images of Vega after different refinements of the adjustment.

in figure 3.3(c). The final figure 3.3(d) shows the spot after activating also the second correction for the parabolic shape of the mirror dish. Fitting again a 2dim gauss to the star image, one gets $\sigma = 11.1,\ 9.2,\ 6.5,\ 5.7$ (CCD pixels) respectively.

As Vega is a very bright star and the intensity of the central part of the spot is over exposed in the images of figure 3.3, we decided to use Omicron-Andromeda a 3.6 mag star to better assess the size of the PSF. In figure 3.4(a) the star is barely visible on the screen as no corrections have been applied to the laser adjustment. After applying the corrections we clearly see the image of this star in figure 3.4(b). All these images where taken during Moonlight conditions which introduced a quite noticeable background. From these first studies we can conclude that we easily can use stars down to magnitude 4.0 during moonlight and even dimmer stars during dark nights, for the pointing model correction. A first estimate also indicates that 80% of the light is concentrated in the central pixel when focusing at infinity. A

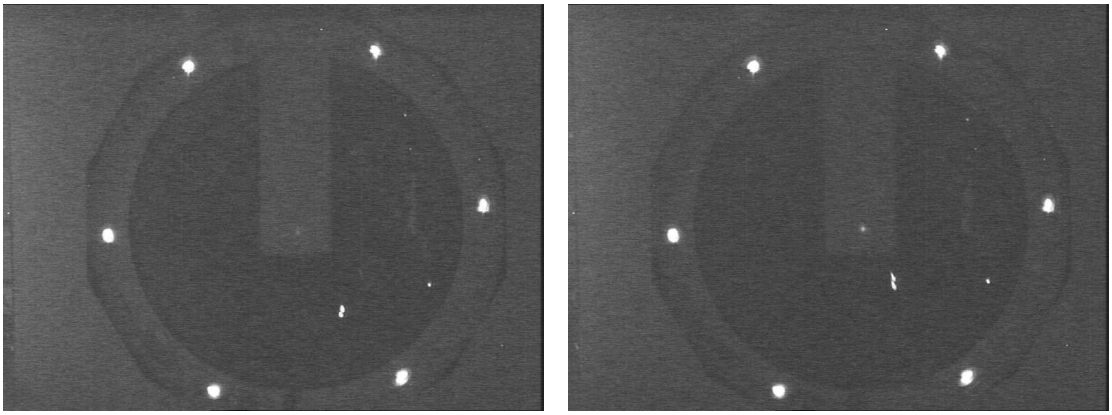

(a) Before corrections

(b) After corrections

Figure 3.4: Images of Omicron Andromedae, a 3.6 mag star.

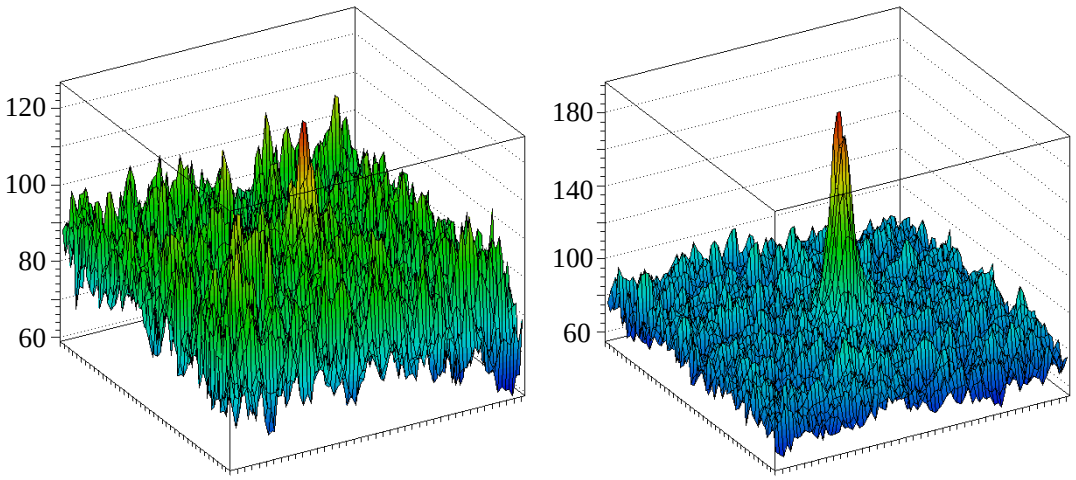

Figure 3.5: Histograms of Omicron Andromedae image (central region) before and after corrections

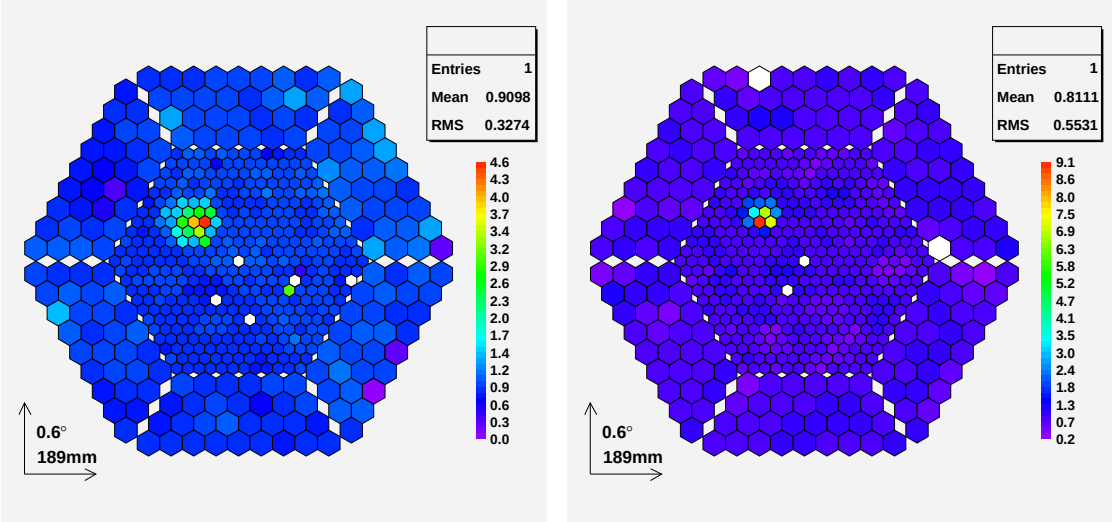

(a) June 2004

(b) August 2004

Figure 3.6: DC Currents obtained while pointing to 3EG J1727+0429.

focusing at 10 km will smear the image more or less by the same amount as due to the wrong focal plane and can be estimated from figure 2.2 to be of the order of 0.4°.

3.3 Analysis of DC-Current files before and after the July installation.

To check that the improvement is also seen in the real data we downloaded some camera control files containing the DC-currents of the PMT camera pixels, which where taken on the 13th of August this year. We selected the field of 3EG-1727+0429 which contains the star 49-Sigma Ophiuchi. This is a very red K3 type star with visual magnitude off 4.3.

The same field was also observed in June so we selected for the comparison a set of observations performed on the 24th of June. For both datasets we calibrated the DC-currents using calibration runs taken with the constant light source. However, not to introduce errors, we did not use the CL runs taken for this field of view but CL runs taken the same night off the field Off-PSR1957-1 for the June data and Off-PSR1951-1 for the August data. Both fields are on quite bright galactic patches of the sky, but don't contain bright stars in the inner part of the camera.

In figure 3.6 we compare the DC current images obtained in both cases. Clearly the august image is much more concentrated and most of the light is in a few pixels. Taken into account the blurring due to the 10 km height focusing, this confirms our estimate that the PSF is now better then 1 PMT pixel for infinity focusing.

We also rescaled the August image, to show the tails of the psf. This can be

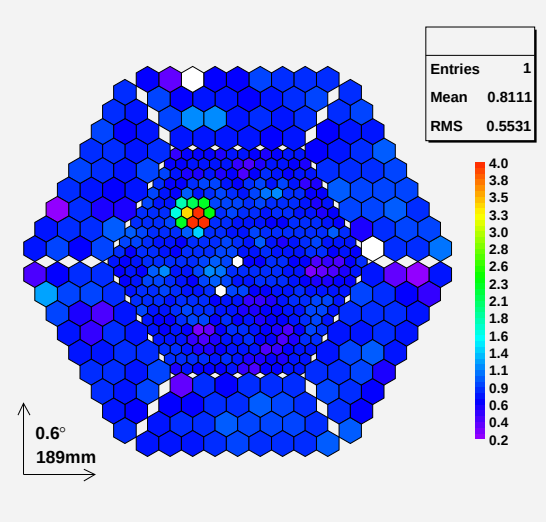

Figure 3.7: DC Currents obtained while pointing to 3EG J1727+0429. Here we rescalled the August data to a maximum of 4 to show the tails of the PSF.

seen in figure 3.7. Some halo, as seen on the CCD images can now be seen in the DC-current image. Also clear indication of some coma effects are visible on the image.

Chapter 4

Next steps and important tasks for the future

4.1 Solving the compiler problem for the ATMEL AVR Microcontrollers

The new CodeVision AVR compiler introduces some timeout errors in the AMC controller cards, which raise the error rate for the panels connected to these controllers to unacceptable levels. On the on side, we can't reprogram the controllers with a new versions of the controller software, which we know solves at least some if not all the communication problems still found with some card containing the old software. On the other side, we can't use the newly produced spare cards which contain a new microcontroller (ATmega16) which can't be programmed with the old compiler versions.

4.2 Improving the determination of the optical axis

The determination of the exact center of the camera to sub-CCD-pixels was not possible in the current configuration. We propose to build a 'focusing central pixel' which contains a exactly positioned LED surrounded by reflective white material at the winston cone plane. The LED can be used to determine the camera center to high accuracy.

4.3 Better CCD camera for the fine focussing of mirrors

A CCD camera with better dynamic range mounted on the temporary camera mast is needed to be able to fine adjust the individual mirrors on each panel to a higher precission. With the used camera not all individual mirrors could be aligned because they may not be fully illuminated and the resulting spot was very weak.

4.4 Better precission focusing of the mirror panels

To improve the now somewhat arbitrary way of focussing individual mirror panels, we recommend to build a special central pixel containing a segmented PIN-Diode so that the optimal focus position can be found finding the position where the signals from each PIN-Diode quadrant reach same strength.

4.5 Higher order corrections in the AMC software

Higher order corrections to the AMC software may be applied. Precise($< 1\%$) knowledge of the distance to the Roque-Lamp can be used to improve the correction calculation.

In a similar way knowledge of the precise position of all mirror panels may improve the correction calculation.